

25 **ABSTRACT**

26 **Global warming during the Paleocene Eocene Thermal Maximum (PETM) ~55**
27 **million years ago (Ma) coincided with a massive release of carbon to the ocean-atmosphere**
28 **system, as indicated by carbon isotopic data. Previous studies have argued for a role of**
29 **changing ocean circulation, possibly as a trigger or response to climatic changes. We use**
30 **neodymium (Nd) isotopic data to reconstruct short high-resolution records of deep-water**
31 **circulation across the PETM. These records are derived by reductively leaching sediments**
32 **from seven globally distributed sites to reconstruct past deep ocean circulation across the**
33 **PETM. The Nd data for the leachates are interpreted to be consistent with previous studies**
34 **that have used fish teeth [Nd isotopes](#) and benthic foraminiferal $\delta^{13}\text{C}$ to constrain regions of**
35 **convection. There is some evidence from combining Nd isotope and $\delta^{13}\text{C}$ records that the**
36 **three major ocean basins may not have had substantial exchanges of deep waters. If the**
37 **isotopic data are interpreted within this framework, then the observed pattern may be**
38 **explained if the strength of overturning in each basin varied distinctly over the PETM,**
39 **resulting in differences in deep-water aging gradients between basins. Results are**
40 **consistent with published interpretations from proxy data and model simulations that**
41 **suggest modulation of overturning circulation had an important role for [initiation and](#)**
42 **recovery of the ocean-atmosphere system [associated with](#) the PETM.**

43

44

45 **1.0 Introduction**

46 The PETM represents a time of profound global change with deep sea temperatures
47 increasing 4-8°C (Katz et al., 1999; Kennett and Stott, 1991; Sluijs et al., 2006; Tripathi and
48 Elderfield, 2004, 2005; Zachos et al., 2001, 2003, 2006), widespread biological extinctions (e.g.
49 Kennett and Stott, 1991), and ocean acidification marked by widespread carbonate dissolution
50 occurring ~ 55 Ma (Dickens, 2000; Kump et al. 2009; Ridgwell and Schmidt, 2010; Zachos et
51 al., 2005, 2008; Zeebe and Zachos, 2007). In general, the timing and global distribution of
52 temperature records across the PETM are consistent with strong greenhouse forcing (Kennett and
53 Stott, 1991; Tripathi and Elderfield, 2004, 2005; Zachos et al., 2001, 2003; Sluijs et al., 2007)
54 although the amount of carbon released, the type of carbon (Zeebe et al., 2009), and the possible
55 role of other forcing agents (e.g., water vapor, aerosol loading, surface albedo feedbacks) is
56 unclear (Bowen et al., 2004; Lunt et al., 2012). Changes in deep ocean circulation, orbital cycles,
57 and volcanic exhalations are proposed causes of the initial warming (e.g., Kennett and Stott,
58 1991; Bice and Marotzke, 2002; Dickens et al., 1995; Lunt et al., 2011, 2012; McInerney and
59 Wing, 2011 Nunes and Norris, 2006; Sluijs et al., 2007; Tripathi and Elderfield, 2005; Winguth et
60 al., 2010; Zachos et al., 2001). Climate simulations even suggest that the magnitude and pacing
61 of the PETM and subsequent smaller events (ETM2 and ETM3) can be explained by orbitally
62 induced changes in water temperature and circulation controlling the destabilization of methane
63 hydrates (e.g. Lunt et al., 2010).

64 A striking characteristic of the PETM is a pronounced global negative stable carbon
65 isotope ($\delta^{13}\text{C}$) excursion (CIE) (Kennett and Stott, 1991; Koch et al., 1992; Bowen et al., 2001;
66 Nunes and Norris, 2006; McCarren et al., 2008; McInerney and Wing, 2011; Zachos et al.,
67 2001). This isotopic excursion resulted from a rapid release (in less than 10,000 years) of carbon

68 from an isotopically light reservoir, likely resulting from the warming climate (e.g., Farley and
69 Eltgroth, 2003; Murphy et al., 2010; Röhl et al., 2007). Based on basinal gradients of available
70 benthic $\delta^{13}\text{C}$ data (Nunes and Norris, 2006; Tripathi and Elderfield, 2005), widespread carbonate
71 dissolution (Dickens, 2000; Kump et al. 2009; Ridgwell and Schmidt, 2010; Zachos et al., 2005,
72 2008), inferred deep-sea carbonate ion gradients (Zeebe and Zachos, 2007), as well as numerical
73 modeling studies (Bice and Marotzke, 2002; Lunt et al., 2012), it has been argued that a change
74 in thermohaline circulation may have been associated with the PETM. Such studies have
75 postulated circulation regimes fundamentally different than the modern ocean operating before
76 and after the PETM (Kennett and Stott, 1991, Lunt et al., 2011). Specifically, studies have
77 proposed the existence of Southern Ocean deep-water formation (Kennett and Stott, 1991) based
78 on high-resolution carbon isotope records that are used to infer basinal deep-water aging
79 gradients (Nunes and Norris, 2006; Tripathi and Elderfield, 2005) and have suggested intermittent
80 deep water formation in the North Pacific based on a fully coupled atmosphere-ocean general
81 circulation model based on pCO_2 simulations (Lunt et al., 2011). It is hypothesized that due to
82 gradual changes in the temperature and hydrology of high-latitude surface waters, these
83 southern-sourced waters were displaced during the PETM with the development of convection in
84 the northern hemisphere (Bice and Marotzke, 2002; Tripathi and Elderfield, 2005; [Nunes and](#)
85 [Norris, 2006; Alexander et al., 2015](#)). The combination of warmer deep water and circulation
86 changes may have served as a trigger or amplifier of the massive carbon release that resulted in
87 the global CIE, possibly through the destabilization of methane hydrates (e.g. Bice and
88 Marotzke, 2002; Lunt et al., 2011).

89 However, interpreting past benthic $\delta^{13}\text{C}$ records in benthic foraminifera of the PETM as a
90 strict indicator of thermohaline circulation is complicated by possible contributions of

91 fractionated carbon sources (Kurtz et al., 2003), changes in marine productivity (Paytan et al.,
92 2007), deep water carbon export (McCarren et al., 2008), extinction and migration events of the
93 biota, and potential signal loss through dissolution in highly corrosive bottom waters (Alexander
94 et al., 2015; McCarren et al., 2008; Pagani et al., 2006; Zeebe and Zachos, 2007). In contrast,
95 the geochemical cycling of Nd in the oceans allows Nd isotopes to be used as a quasi-
96 conservative tracer of water mass distributions that is generally not affected by biogeochemical
97 processes that can be used to reconstruct past ocean circulation (e.g., Frank, 2002; Goldstein et
98 al., 2003; Thomas, 2004).

99 Published records of past seawater Nd isotope compositions (ϵ_{Nd}) extracted from fossil
100 fish teeth serve as a proxy for past deep-water mass distributions and mixing and do not show
101 | [clear](#) evidence for changes at the PETM. Specifically, the low-resolution ϵ_{Nd} data from fish teeth
102 | have been interpreted as possibly reflecting an uninterrupted contribution from a Southern Ocean
103 deep-water source in multiple basins across the PETM (Thomas et al., 2003). This apparent
104 disparity between proxy data may reflect the non-conservative nature of interpreting benthic
105 foraminiferal $\delta^{13}C$, or could arise from the low-resolution nature of the published Nd isotope
106 records.

107 To address whether there is Nd isotope evidence for changes in water mass distributions,
108 we developed high-resolution records of the ϵ_{Nd} composition of Fe-Mn leachates from seven
109 sites and compare these results to published ϵ_{Nd} data for fish teeth (Thomas et al., 2003) and
110 benthic foraminiferal $\delta^{13}C$ (Nunes and Norris, 2006; Tripathi and Elderfield, 2005; Zachos et al.,
111 2001). The Nd isotope composition of Fe-Mn oxide leachates from core-top sediments has been
112 used to accurately reconstruct bottom water values (Rutberg et al., 2000; Bayon et al., 2002;
113 Gutjahr et al., 2007). This technique has also been applied to downcore sediments to study

114 variations in bottom water circulation during the Pleistocene (Rutberg et al., 2000; Piotrowski et
115 al., 2004, 2005, 2008). Measurements on older sediments ranging from Cenozoic (Martin et al.,
116 2010) to Cretaceous (Martin et al., 2012) in age has shown that sequences from multiple
117 localities can preserve a Nd isotope signal similar to fish teeth and can be used to develop high-
118 resolution paleoceanographic records.

119

120 **2. Materials and Methods**

121 *2.1 Sample and locality information*

122 Details on the core locations, depths and paleo-depths are given in Table 1. Sites were
123 located at similar water depths during the PETM, with paleodepths between 2400 and 3200 m in
124 the Pacific, between 1900 and 2000 m in the North Atlantic, and between 1900 and 3400 m in
125 the Southern and Indian Oceans (Table 1). Sources for the carbon isotope data referred to in this
126 study is reported in this table. The age models used to plot all the data (including $\delta^{13}\text{C}$) are
127 shown in Table 2, and are derived from the information given in the publications of the $\delta^{13}\text{C}$ data
128 (Thomas et al., 2003; Nunes and Norris, 2006; Tripathi and Elderfield, 2005). For completeness,
129 we show in Table 2 the core depth-age curve fits that describe the age models for each core,
130 where:

$$131 \text{Age (Myr)} = m(\text{Core Depth in mbsf}) + b.$$

132 Several segments are listed if sedimentation rates varied down core (the depth ranges of
133 these segments are listed in Table 2). In all cases, simple linear sedimentation rates were used.
134 These age models were also used to calculate the ages used here for the fish teeth/debris data
135 (Thomas et al., 2003).

136

137 2.2 Sample preparation

138 Freeze-dried sediment samples were obtained from the Integrated Ocean Drilling
139 Program (IODP). One to two grams dry weight of sediment was then rinsed with ultra-high
140 purity (Milli-Q) water, and then processed following established sediment leaching protocols
141 (e.g., Bayon et al., 2002, 2004; Haley et al., 2008a; Jacobsen and Wasserburg, 1979; Martin et
142 al., 2010; Piotrowski et al., 2008; Rutberg et al., 2000; Scher and Martin, 2006). Briefly, we
143 thoroughly rinse the sediments with Milli-Q water, leach with buffered acetic acid for 2.5 hours
144 and collect the leachate, then rinse thoroughly with Milli-Q again before the reduction of early
145 diagenetic metal oxide coatings that carry the bottom water Nd isotope signatures with a dilute
146 buffered hydroxylamine.HCl-acetic acid solution. This buffered hydroxylamine.HCl-acetic acid
147 solution leaches the authigenic metal oxide coatings, which are then removed from the sediment
148 and run through standard chromatographic procedures to extract a pure Nd solution for mass
149 spectrometric analyses (AG 50W X12 resin for cation separation followed by di-2-ethylexyl-
150 phosphate resin for rare earth element separation; see Gutjahr et al. 2007 for details). The
151 reliability of these signatures is supported by recent publications demonstrating the validity of
152 hydroxylamine.HCl leaches in the absence of volcanic material (e.g. Khélifi and Frank, 2014;
153 Böhm et al., 2015). Potential uncertainties are associated with leaching sediments that may have
154 undergone late stage diagenesis, although to our knowledge no [particular](#) examples exist in the
155 literature for the influence of late stage diagenesis on the recorded ϵ Nd signature. For this reason
156 we focus our interpretations on the relative changes in the Nd isotope signature rather than on
157 absolute values.

158

159 2.3 Sample analysis

160 Nd was analyzed on two instruments: a Triton Thermal-Ionization Mass Spectrometer at
161 IFM-GEOMAR, using $^{146}\text{Nd}/^{144}\text{Nd} = 0.7219$ to correct for instrument fractionation, and a Nu
162 Instruments multi-collector inductively coupled mass spectrometer at Oregon State University.
163 Nd isotopes are expressed in ϵ_{Nd} notation, defined as the deviation of measured $^{143}\text{Nd}/^{144}\text{Nd}$ ratios
164 from a bulk Earth value of CHUR (chondritic uniform reservoir) in the 5th decimal place
165 (Thomas et al., 2003). Long-term reproducibility of a Nd standard solution (SPEX source) gave a
166 2σ error of $0.5 \epsilon_{\text{Nd}}$ units representing the total error of analyses and normalization, exactly as the
167 samples. Analyses of the JNdi standard used for normalization had a lower 2σ error of $0.3 \epsilon_{\text{Nd}}$
168 units. Nd isotope data are not corrected for decay of samarium given the limited temporal range
169 of the data and the lack of constraints on sample Sm/Nd isotope ratios. Nd isotope corrections for
170 the PETM are typically small ($<0.5 \epsilon_{\text{Nd}}$ units; Thomas et al. 2003) and therefore do not influence
171 our interpretations.

172

173 **3. Results and Discussion**

174 We have applied a leaching technique (Gutjahr et al., 2007; Haley et al., 2008a; Haley et
175 al., 2008b; Rutberg et al., 2000) that allows the extraction of past bottom water Nd isotope
176 compositions from the Fe-Mn oxide component of marine sediments, expressed as ϵ_{Nd} units
177 (Jacobsen and Wasserburg, 1979). Such data provide high-resolution records of changes in past
178 deep-water mass mixing and [are used to reconstruct deep ocean](#) circulation ([Böhm et al., 2015;](#)
179 [Martin et al., 2010, 2012; Piotrowski et al., 2004, 2005, 2008; Thomas et al., 2014](#)). [Here](#) we
180 compare [deep water Nd isotope data obtained](#) from leachates [to fish teeth records and](#) carbon
181 isotope data from the same cores, [which allows us](#) to elucidate the causes and controls of $\delta^{13}\text{C}$
182 variations in the past deep oceans (Piotrowski et al., 2005). Our new Nd [isotope](#) data are

183 combined with existing $\delta^{13}\text{C}$ records and published Nd isotope data from fossil fish teeth of the
184 Atlantic, Indian and Southern Oceans (Thomas et al., 2003), in order to obtain a reconstruction
185 of Nd isotope distributions, and thus deep ocean circulation, for all major ocean basins across the
186 PETM at a resolution comparable to the corresponding $\delta^{13}\text{C}$ data (Figure 1).

187

188 *3.1 Comparison of neodymium isotope data obtained using different archives*

189 Consistent with published results for a number of different sedimentary environments
190 (Martin et al., 2012), we find a general agreement (Figure 1) between Nd isotopic data from
191 sediment leaches and fish teeth (Thomas et al., 2003): there does appear to be a small systematic
192 offset between these data at Sites 401 and 690B. This offset may be the result of a temporal
193 difference between uptake or retention of Nd in teeth and the ferromanganese coatings during
194 sedimentation and diagenesis, or of higher-order variability at these locations, or a combination
195 of the two. Regarding the latter, model studies (Lunt et al., 2011; Winguth et al., 2010) have
196 confirmed that locations near the Antarctic continent, such as at Site 690B, were sensitive to
197 changes in climate conditions, and, as such, likely to have varied more substantially during the
198 PETM (55.14-55.23 Ma for this study based on the CIE; Figure 1). Due to limited constraints to
199 explain the offsets between fish teeth and leach records in detail, we focus our interpretations on
200 the relative trends and broader patterns of the ϵ_{Nd} signatures over time and their relation to the
201 CIE rather than on absolute values.

202

203 *3.2 Basin-wide changes of deep water Nd isotope compositions*

204 The overall patterns in our records support previous studies that have inferred convection
205 patterns in the Southern Ocean and in both the North and South Pacific during the PETM. Our

206 ϵ_{Nd} records cover the three major ocean basins (Figure 1) and reveal distinct and basin-specific
207 changes in deep circulation across the PETM. These data suggest that a change in ocean
208 circulation may have triggered the carbon release associated with the PETM; in particular Pacific
209 Site 1220 is key in that it shows variance of up to $\sim 2 \epsilon_{Nd}$ units prior to the CIE (Figure 2) while
210 fish teeth ϵ_{Nd} records indicate a similarly sized excursion in the Southern Ocean.

211 Southern Ocean Sites 527 (subtropical South Atlantic) and 690 (Atlantic sector of the
212 Southern Ocean) fluctuated (1 to 1.3 ϵ_{Nd} units) around a mean ϵ_{Nd} signature of ~ -9 throughout
213 the record, with indications of a shift to in-phase co-variation during and after the PETM, also
214 reflected by the evolution of Site 213 (Figure 1). The ϵ_{Nd} records for eastern North Atlantic Site
215 401 stabilize at ~ -9.3 during the PETM and then at ~ -8.2 post-PETM, with the trend towards
216 more radiogenic values occurring at the end of the PETM. While the fish teeth ϵ_{Nd} record is not
217 a step-function, the observed magnitude and direction of change in leachate ϵ_{Nd} signatures is
218 consistent with those changes reported from fish teeth ϵ_{Nd} signatures (Thomas et al., 2003)
219 (Figure 1, 2). Deep waters at central (western) Atlantic Site 1051B, located near the proto-
220 Caribbean, had a more positive ϵ_{Nd} (~ -8) than Site 401 prior to the PETM, but post-PETM ϵ_{Nd}
221 signatures at both sites converged (Figure 1). The record of Site 1051B exhibits similarities to
222 post-PETM data from Site 401, which could indicate greater mixing within the North Atlantic
223 following PETM recovery (Figure 1). Pacific sites 1209B and 1220B were more radiogenic than
224 the other basins (ϵ_{Nd} from -6 to -2). With the exception of one data point ($-2.1 \epsilon_{Nd}$ at 55.02 Ma),
225 the western Pacific (Site 1209B) had a remarkably constant ϵ_{Nd} signature of -3.7 pre- and post-
226 PETM (Figure 1). In contrast, the eastern Pacific (Site 1220B) ϵ_{Nd} shows variance from ~ -4 to

227 $\sim -5.5 \epsilon_{Nd}$ prior to and during the PETM, before stabilizing after the PETM at ϵ_{Nd} of ~ -5 (Figure
228 1, 2).

229

230 *3.3 A conceptual model to explain the records*

231 The dissimilarities between the ϵ_{Nd} records confirm that the globally consistent CIE
232 dominantly reflects a change in the source of oceanic carbon (Thomas et al., 2002). This change
233 is not directly from a volcanic or extra-terrestrial source, as these would also be seen the ϵ_{Nd}
234 records (Cramer and Kent, 2005). However, the ϵ_{Nd} data also clearly indicate that changes in
235 water mass distributions and mixing were associated with the PETM and suggest a
236 fundamentally different circulation patterns existed during this period of time. Without such
237 changes in circulation, we would expect that the ϵ_{Nd} signals remained constant over the entire
238 record or only show a slow and predictable trend that reflects changes on geological time scales
239 (e.g. the evolution of weathering inputs as opposed to more rapid oceanic changes). Figure 3
240 illustrates our hypothetical reconstruction of the evolution of global deep-water mass exchange
241 during the PETM, based on the interpretation of the global ocean as three distinct deep-water
242 basins: the “Southern Ocean,” the North Atlantic and the Pacific. While in this model we
243 hypothesize the basins only had restricted water mass exchange between them, we cannot
244 eliminate the possibility of unrestricted exchange since similar scale inter-basinal differences in
245 ϵ_{Nd} are observed in the modern ocean without this restriction. That is, the modern North Atlantic
246 Deep Water signature increases by $\sim 1.5 \epsilon_{Nd}$ unit from the the North ($-13.5 \epsilon_{Nd}$) to South Atlantic
247 ($-12 \epsilon_{Nd}$; Lacan et al., 2012) due to mixing, which is a similar magnitude as the offset observed in
248 our data ($\sim 1 \epsilon_{Nd}$ unit).

249 | [Our interpretation of these](#) $\delta^{13}\text{C}$ and ϵ_{Nd} data supports changes in areas of convection that
250 | are consistent with simulations of the PETM with coupled climate models (Lunt et al., 2012,
251 | Thomas et al., 2014) and with a comprehensive climate model (Winguth et al., 2010). It is
252 | impossible to interpret from the Nd isotope data alone whether there was reduced or increased
253 | overturning associated with carbon release, as these data reflect water mass geometries and not
254 | rates of overturning. It is of note that model simulations support a weakening of the meridional
255 | overturning circulation with increased greenhouse gases, which might result in a water mass
256 | geometry similar to what is reconstructed. However, changes in the exchange between ocean
257 | basins will be dependent on several factors, including buoyancy-induced and wind-stress induced
258 | changes in overturning, as well as topography. Below we discuss whether there is evidence for
259 | changes in ventilation from basinal deep-water aging gradients, and what the nature of
260 | topographic barriers may have been to produce the observed patterns in the data.

261

262 | 3.3.1. Southern *Ocean* records

263 | An ϵ_{Nd} signature of -9.2 in the “Southern Ocean” most likely reflects an Antarctic margin
264 | source, similar to present day Antarctic-sourced intermediate waters (Stichel et al., 2012;
265 | Thomas et al., 2003). In agreement with previous inferences from $\delta^{13}\text{C}$ data (Tripathi and
266 | Elderfield, 2005; Zeebe and Zachos, 2007), such a deep-water source can readily explain the
267 | post-PETM similarity of the ϵ_{Nd} records from both the Southern Atlantic (Site 527) and Indian
268 | Ocean (Site 213) with the Atlantic sector of the Southern Ocean (Site 690) (Figures [1](#), [3](#)). There
269 | are indications that the co-variation of ϵ_{Nd} at Sites 213, 527, and 690 was enhanced immediately
270 | before, during, and following the PETM, which [is](#) consistent with [an](#) intensification of Southern
271 | Ocean-sourced ventilation (Figure [1](#), 2a) [that systematically affected all sites](#).

272 | The ϵ_{Nd} signatures from fish teeth from site 690 and 527 suggest rapid changes in
273 | circulation leading into and during the early part of the PETM (Figure 2). The previously
274 | proposed formation of low-latitude Tethyan deep-water (e.g., Cope and Winguth, 2011; Huber
275 | and Sloan, 2001), or slower overturning circulation (Winguth et al., 2010) are unlikely to have
276 | generated such a range and similarity in the evolution of ϵ_{Nd} signatures at these three sites.
277 | Furthermore, numerical simulations indicate that strong overturning circulation with multiple
278 | deep convection sites best explains the ϵ_{Nd} record (Thomas et al., 2014).

279

280 | 3.3.2. Atlantic Ocean records

281 | The contrast in ϵ_{Nd} trends between the Southern Ocean and those of the North Atlantic
282 | (Figure 2) indicates that there was little exchange between these basins. The young Mid-
283 | Atlantic Ridge (MAR) between Africa and South America most likely represented an efficient
284 | barrier for north-south intermediate and deep-water exchange (Bice and Marotzke, 2002). This
285 | differs from previous interpretations of overturning circulation in the Atlantic (Bice and
286 | Marotzke, 2002; Nunes and Norriz, 2006; Thomas et al., 2003), but confirms recent modeling
287 | results (Winguth et al., 2010). The differences between the two North Atlantic ϵ_{Nd} records can be
288 | readily explained by a weak North Atlantic deep-water overturning cell, resulting in higher
289 | sensitivity to local changes in Nd inputs or locally variable deep-water mass circulation.
290 | Assuming weak, low-latitude, halothermally-driven downwelling in the North Atlantic basin, we
291 | would expect Site 401 to show an ϵ_{Nd} evolution different from Site 1051B, which is indeed
292 | documented in Figure 2c. The contrasting North Atlantic ϵ_{Nd} records (Figure 2c) also support
293 | model predictions (Winguth et al., 2010) that the North Atlantic was well-stratified until after the

294 | PETM, which is reflected by the [later](#) convergence of the Nd isotope records indicating more
295 | efficient vertical [and basinal](#) mixing ([Figure 1](#)). [Pre-PETM](#) stratification was potentially
296 | interrupted briefly near the onset of the PETM. Specifically, ϵ_{Nd} signatures [of](#) fish teeth from site
297 | 401 indicate [that](#) the Atlantic may have experienced rapid circulation change early in the PETM
298 | ([Figure 2c](#)) with ϵ_{Nd} briefly shifting from ~ -9 to ~ -10 .
299 |

300 | 3. 3.3. Pacific Ocean records

301 | The distinct ϵ_{Nd} records of the Pacific point to restricted Pacific intermediate water mass
302 | exchange with the “Southern Ocean” ([Figure 3](#)). [A](#) possible barrier preventing substantial
303 | exchange between the Southern Ocean and Pacific Ocean [were](#) the shallow seas between
304 | southern Asia and Australia (Bice and Marotzke, 2002). Within the Pacific Ocean, times of
305 | convergent ϵ_{Nd} can be explained by a weakened southern Pacific ventilation which would allow
306 | northern Pacific water to influence both sites. [Conversely, with](#) intensified Southern Ocean
307 | sourced ventilation, [the \$\epsilon_{Nd}\$ signature of deep waters at](#) Pacific Site 1220B would have diverged
308 | from the signatures of the northern source (Bice and Marotzke, 2002).

309 | It follows that a Pacific circulation pattern consistent with both $\delta^{13}C$ and ϵ_{Nd} data must
310 | involve distinct southern- and northern-Pacific sources of deep waters, as predicted in previous
311 | studies (Lunt et al., 2011; Thomas, 2004; Thomas et al., 2008; Winguth et al., 2010). [While we](#)
312 | [unfortunately lack samples prior to 55.25Ma, there is high variability](#) in the ϵ_{Nd} record at site
313 | 1220 immediately prior to [and at the beginning of](#) the PETM ([based on the CIE timing](#)) [that](#) may
314 | reflect sudden [and short-lived intensification in](#) deep-water formation in the North Pacific
315 | ([Figure 2, 3](#)). The initial change in ϵ_{Nd} from ~ -4 to ~ -6 at Site 1220B [clearly occurred](#)

316 stratigraphically below the negative CIE, consistent with the hypothesis that circulation changes
317 triggered PETM carbon release.

318 Alternative scenarios are that the more negative ϵ_{Nd} at the beginning of the PETM reflects
319 a dramatic change in ventilation from a southern source that occurred just prior to the PETM,
320 possibly accompanied by a change in deep-ocean redox conditions leading to diagenetic
321 alteration of the Nd isotope record. However, several lines of evidence suggest the negative Nd
322 isotope "excursion" at the start of the PETM reflects changes in bottom water sourcing and not
323 changes in the position of a sediment redox front. First, a ventilation change in the deep Pacific
324 is in agreement with interpretations of carbon isotope data that support a reversal or large change
325 in deep-water aging gradients between basins (Tripathi and Elderfield, 2005). Secondly, there are
326 carbonate geochemical data that suggest a reversal or dramatic change in deep ocean carbonate
327 saturation gradients between basins, consistent with a major circulation change (Zeebe and
328 Zachos, 2007). Thirdly, substantially larger redox changes are observed in PETM sequences
329 from other basins (i.e., the South Atlantic; Chun et al., 2010) that do not exhibit similar
330 corresponding shifts in records of ϵ_{Nd} . Fourthly, similar types of changes are observed during
331 Cretaceous ocean anoxic events (Martin et al., 2012) where there also is no unequivocal evidence
332 for redox fronts biasing the sediment leachate ϵ_{Nd} record. Finally, core photographs show that
333 transitions in sediment redox at Site 1220B are not directly coincident with the ϵ_{Nd} change.

334 Thus we conclude our Nd isotope data are consistent with other proxy data (Nunes and
335 Norris, 2006; Tripathi and Elderfield, 2005; Zeebe and Zachos, 2007) and models (Bice and
336 Marotske, 2002; Lunt et al, 2011) and reflect a circulation change at the PETM. These data
337 indicate a Pacific circulation ‘trigger’ for carbon release, the record of which is, as predictable,
338 most pronounced in the Pacific Ocean. Some simulations indicate that at the PETM a change in

339 | state of a Southern Pacific deep-water source may have contributed to hydrate destabilization,
340 | which these data may reflect; such changes in Southern Ocean water mass characteristics could
341 | ultimately have arisen from a gradual forcing such as volcanic outgassing (Kennett and Stott,
342 | 1991; Bice and Marotske, 2002; Lunt et al., 2011; Tripathi and Elderfield, 2005).

343 | One outstanding feature in our data is the mode of circulation during and after the PETM.
344 | As depicted in Figure 3, our data suggest that the circulation pattern prior to the ϵ_{Nd} "excursion"
345 | was similar to that prevailing during the PETM. In contrast the "trigger" circulation mode (i.e.,
346 | during the "excursion" itself) was similar to the mode of circulation after the PETM. While it is
347 | unfortunate that no additional samples are available from site 1220B to further investigate these
348 | trends, we have confidence that they are representative of the changes that occurred given that
349 | more than one data point defines each part of the "excursion" (Figure 2a). In essence, our
350 | interpretation simply implies that deep ocean circulation in the Pacific switched between two
351 | modes during this period of time. That the ϵ_{Nd} data of sites 1220B and 1209 are similar prior to
352 | the "excursion" and that the ϵ_{Nd} of site 1220B appears to be bimodal (at ~ -5.5 and ~ -4.5) is
353 | consistent with the idea of two distinct circulation patterns. The fact that the CIE was a transient
354 | pulse reflective of the source function of the carbon is not inconsistent with our interpretations
355 | presented here.

356

357 | **CONCLUSIONS**

358 | Our study provides new neodymium isotope data from Fe-Mn leachates constraining
359 | changes in ocean circulation associated with the PETM. The novelty of these Nd isotope data
360 | reflect advances in our ability to extract such data from pelagic sediments, which has opened
361 | new avenues of paleoceanographic research. Using Nd isotopes, a proxy independent of carbon

362 cycle processes, we unravel oceanographic changes during the PETM and are able to isolate
363 competing factors controlling the carbon-isotope record during the PETM. In general, we find
364 these data are similar to results from fish teeth (a more widely used proxy), and discuss the
365 combined high-resolution records for seven sites.

366 The high-resolution combined Nd isotope records provide further evidence for changes in
367 thermohaline circulation associated with the PETM, as previously inferred from basinal carbon
368 isotope gradients (Nunes and Norris, 2006; Tripathi and Elderfield, 2005) and constraints on deep-
369 water carbonate ion concentrations (Zeebe and Zachos, 2007). In addition, these new records
370 provide additional constraints on the timing and the nature of changes in circulation. The records
371 are consistent with variations in bottom water mass mixing in each basin associated with the
372 PETM, with water mass distributions implying intermediate and deep-water circulation changes.
373 We find that changes in deep ocean circulation occurred during the Paleocene-Eocene, and that
374 these circulation changes likely preceded the carbon release, based on ϵ_{Nd} shifts observed
375 stratigraphically below the carbon isotope excursion. Together with modeling results (Bice and
376 Marotzke, 2002; Lunt et al., 2011, 2012; Winguth et al., 2010) and Mg/Ca-based bottom water
377 temperature estimates (Tripathi and Elderfield, 2005), Nd isotope data provide further evidence
378 for thermohaline changes that may have served as a “trigger” of carbon release.

379

380 **ACKNOWLEDGEMENTS**

381 Samples were provided by the Integrated Ocean Drilling Program. NSF grant 1147407 supported
382 the contributions of A.N.A. A.T. was supported by a NERC Fellowship, a Junior Research
383 Fellowship from Magdalene College, and the UCLA Division of Physical Sciences, and thanks
384 Alex Piotrowski for discussing this work and making some pilot measurements. C. Teschner, R.

385 Stumpf and J. Heinze are acknowledged for laboratory support and F. Hauff is thanked for
386 technical support of the mass spectrometer at GEOMAR, Kiel. This work was also supported by
387 the "Laboratoire d'Excellence" LabexMER (ANR-10-LABX-19) and co-funded by a grant from
388 the French government under the program "Investissements d'Avenir".

389

390 **REFERENCES CITED**

391

392 Alexander, K., Meissner, K.J., Bralower, T.J., 2015. Sudden spreading of corrosive bottom
393 water during the Palaeocene-Eocene Thermal Maximum. *Nat. Geo.*, **8**, 458-462. DOI:
394 10.1038/NGEO2430.

395 Bayon, G., German, C., Boella, R., Milton, J., Taylor, R., Nesbitt, R., 2002. An improved
396 method for extracting marine sediment fractions and its application to Sr and Nd isotopic
397 analysis. *Geochim. Cosmochim. Acta*, v. 187, p. 170–199.

398 Bayon, G., German, C.R., Burton, K.W., Nesbitt, R.W., & Rogers, N., 2004. Sedimentary Fe-
399 Mn oxyhydroxides as paleoceanographic archives and the role of Aeolian flux in regulating
400 oceanic dissolved REE. *Earth and Planetary Science Letters*, v. 224, p 477-492, doi:
401 10.1016/j.epsl.2004.05.033

402 Bice, K.L. & Marotzke, J., 2002, Could changing ocean circulation have destabilized methane
403 hydrate at the Paleocene/Eocene boundary? *Paleoceanography*, v. 17, p.1018,
404 doi.10.1029/2001pa000678.

405 Böhm, E., Lippold, J., Gutjahr, M., Frank, M., Blaser, P., Antz, B., Fohlmeister, J., Frank, N.,
406 Andersen, M.B., & Deininger, M., 2015. Strong and deep Atlantic meridional

407 overturning circulation during the last glacial cycle. *Nature*, v.517, doi:
408 10.1038/nature14059

409 Bowen, G. J., Beerling, D. J., Koch, P. L., Zachos, J. C., & Quattlebaum, T., 2004. A humid
410 climate state during the Palaeocene/Eocene thermal maximum. *Nature*, v. 432(7016), p. 495-
411 499.

412 Bowen, G. J., Koch, P. L., Gingerich, P. D., Norris, R. D., Bains, S., & Corfield, R. M., 2001.
413 Refined isotope stratigraphy across the continental Paleocene-Eocene boundary on Polecat
414 Bench in the northern Bighorn Basin. *Paleocene-Eocene stratigraphy and biotic change in
415 the Bighorn and Clarks Fork basins, Wyoming. University of Michigan Papers on
416 Paleontology*, v. 33, p. 73-88.

417 Chun, C. O., Delaney, M. L., & Zachos, J. C., 2010. Paleoredox changes across the Paleocene-
418 Eocene thermal maximum, Walvis Ridge (ODP Sites 1262, 1263, and 1266): Evidence from
419 Mn and U enrichment factors. *Paleoceanography*, 25(4), DOI: 10.1029/2009PA001861.

420 Cope, J.T. & Winguth, A., 2011, On the sensitivity of ocean circulation to arctic freshwater input
421 during the Paleocene/Eocene Thermal Maximum. *Palaeogeography, Palaeoclimatology,
422 Palaeoecology*, v. 306, p. 82-94.

423 Cramer, B.S. & Kent, D.V., 2005, Bolide summer: The Paleocene/Eocene thermal maximum as
424 a response to an extraterrestrial trigger. *Palaeogeography, Palaeoclimatology,
425 Palaeoecology*, v. 224, p. 144-166, doi.10.1016/J.Paleo.2005.03.040.

426 Dickens, G.R., O'Neil, J.R., Rea, D.K., & Owen, R.M., 1995, Dissociation of oceanic methane
427 hydrate as a cause of the carbon isotope excursion at the end of the Paleocene.
428 *Paleoceanography*, v. 10, p. 965-971.

429 Dickens, G.R., 2000. Methane oxidation during the late Paleocene thermal maximum. *Bulletin*
430 *de la Société Géologique de France*, v. 171, p. 37-49.

431 Farley, K.A. & Eltgroth, S.F., 2003, An alternative age model for the Paleocene-Eocene thermal
432 maximum using extraterrestrial ³He. *Earth and Planetary Science Letters*, v. 208, p.135-148.

433 Frank, M., 2002, Radiogenic isotopes: Tracers of part ocean circulation and erosional input.
434 *Review of Geophysics*, v. 40(1), p.1001, doi.10.1029/2000RG000094.

435 Goldstein, S.L., Hemming, S.R., Heinrich, D.H., & Karl, K.T., 2003, Long-lived Isotopic
436 Tracers in Oceanography, Paleoceanography, and Ice-sheet Dynamics. *Treatise on*
437 *Geochemistry* (ed. Elderfield, H.) 453-489.

438 Gutjahr, M., *et al.*, 2007, Reliable extraction of a deepwater trace metal isotope signal from Fe-
439 Mn oxyhydroxide coatings of marine sediments. *Chemical Geology*, v. 242, p. 351-370,
440 doi.10.1016/J.Chemgeo.2007.03.021.

441 Haley, B.A., Frank, M., Spielhagen, R.F., & Fietzke, J., 2008a, Radiogenic isotope record of
442 Arctic Ocean circulation and weathering inputs of the past 15 million years.
443 *Paleoceanography*, v. 23, doi.10.1029/2007PA001486.

444 Haley, B.A., Frank, M., Spielhagen, R.F., & Eisenhauer, A., 2008b, Influence of brine formation
445 on Arctic Ocean circulation over the past 15 million years. *Nature Geoscience*, v. 1, p. 68-
446 72, doi.10.1038/Ngeo.2007.5.

447 Higgins, J.A. & Schrag, D.P., 2006, Beyond methane: Towards a theory for the Paleocene-
448 Eocene Thermal Maximum. *Earth and Planetary Science Letters*, v. 245, 523-537,
449 doi.10.1016/JEpsl.2006.03.009.

450 Huber, M., & Sloan, L.C., 2001, Heat transport, deep waters, and thermal gradients: Coupled
451 simulation of an Eocene Greenhouse Climate. *Geophysical Research Letters*, v. 28, p. 3481-
452 3484.

453 Jacobsen, S.B. & Wasserburg, G.J., 1979, Mean Age of Mantle and Crustal Reservoirs. *Journal*
454 *of Geophysical Research*, v. 85, p. 7411-7427.

455 Katz, M.E., Pak, D.K., Dickens, G.R., & Miller, K.G., 1999. The source and fate of massive
456 carbon input during the latest Paleocene thermal maximum. *Science*, v. 286, p. 1531-1533.

457 Kennett, J.P. & Stott, L.D., 1991, Abrupt deep-sea warming, palaeoceanographic changes and
458 benthic extinctions at the end of the Palaeocene. *Nature*, v. 353, p. 225-229.

459 Khélifi, N., and Frank, M., 2014. A major change in North Atlantic deep water circulation 1.6
460 million years ago. *Climates of the Past*, v. 10, p 1441-1451. doi 10.5194/cp-10-1441-2014

461 Koch, P. L., Zachos, J. C., & Gingerich, P. D., 1992. Correlation between isotope records in
462 marine and continental carbon reservoirs near the Paleocene Eocene boundary. *Nature*, v.
463 358, p. 319-322.

464 Kump, L., Bralower, T., & Ridgwell, A., 2009. Ocean acidification in deep time.
465 *Oceanography*, v. 22, p 94-107.

466 Kurtz, A.C., Kump, L.R., Arthur, M.A., Zachos, J.C., & Paytan, A., 2003, Early Cenozoic
467 decoupling of the global carbon and sulfur cycles. *Paleoceanography* v. 18, p. 1090,
468 doi.10.1029/2003pa000908.

469 Lacan, F., Tachikawa, K., Jeandel, C., 2012, Neodymium isotopic composition of the oceans: A
470 compilation of seawater data. *Chemical Geology* v 300-301, 177-184.

471 Lunt, D.J., Ridgwell, A., Sluijs, A., Zachos, J., Hunter, S., & Haywood, A., 2011, A model for
472 orbital pacing of methane hydrate destabilization during the Palaeogene. *Nature Geoscience*,
473 v. 4, p. 775-778, doi.10.1038/Ngeo1266.

474 Lunt, D. J., Dunkley Jones, T., Heinemann, M., Huber, M., LeGrande, A., Winguth, A., Loptson,
475 C., Marotzke, J., Roberts, C. D., Tindall, J., Valdes, P., and Winguth, C., 2012, A model-data
476 comparison for a multi-model ensemble of early Eocene atmosphere-ocean simulations:
477 EoMIP, *Clim. Past*, v. 8, p.1717-1736, doi:10.5194/cp-8-1717-2012.

478 Martin, E.E., Blair, S.W., Kamenov, G.D., Scher, H.D., Bourbon, E., Basak, C., and Newkirk,
479 D.N., 2010. Extraction of Nd isotopes from bulk deep sea sediments for paleoceanographic
480 studies on Cenozoic time scales. *Chem. Geol.*, v. 269, p. 414-431.

481 Martin, E.E., MacLeod, K.G., Berrocoso, A.J., & Bourbon, E., 2012. Water mass circulation on
482 Demerara Rise during the Late Cretaceous based on Nd isotopes. *Earth and Planetary*
483 *Science Letters*, v. 327-328, p. 111-120.

484 McCarren, H., Thomas, E., Hasegawa, T., Rohl, U., & Zachos, J.C., 2008, Depth dependency of
485 the Paleocene-Eocene carbon isotope excursion: Paired benthic and terrestrial biomarker
486 records (Ocean Drilling Program Leg 208, Walvis Ridge). *Geochemistry Geophysics*
487 *Geosystems*, v. 9, doi.10.1029/2008gc002116: Q10008.

488 McInerney, F.A., Wing, S.L., 2011. The Paleocene-Eocene Thermal Maximum: A Perturbation
489 of Carbon Cycle, Climate, and Biosphere with Implications for the Future, *Annual Review of*
490 *Earth and Planetary Sciences*, v. 39, p. 489-516.

491 Molina-Kescher, M., Frank, M., and Hathorne, E., 2014. South Pacific dissolved Nd isotope
492 compositions and rare earth element distributions: Water mass mixing versus biogeochemical

493 cycling. *Geochimica et Cosmochimica Acta*, v. 127, p 171-189. doi:
494 10.1016/j.gca.2013.11.038

495 Murphy, B.H., Farley, K.A., & Zachos, J.C., 2010, An extraterrestrial ³He-based timescale for
496 the Paleocene-Eocene thermal maximum (PETM) from Walvis Ridge, IODP Site 1266.
497 *Geochimica et Cosmochimica Acta*, v. 74, p. 5098-5108.

498 Nunes, F. & Norris, R.D., 2006, Abrupt reversal in ocean overturning during the
499 Palaeocene/Eocene warm period. *Nature*, v. 439, p. 60-63, doi.10.1038/Nature04386.

500 Pagani, M., Pedentchouk, N., Huber, M., Sluijs, A., Schouten, S., Brinkhuis, H., Sinnghe-
501 Damste, J., & Dickens, G. R., 2006. Arctic hydrology during global warming at the
502 Palaeocene/Eocene thermal maximum. *Nature*, v. 442(7103), p. 671-675.

503 Paytan, A., Averyt, K., Faul, K., Gray, E., and Thomas, E., 2007, Barite accumulation, ocean
504 productivity, and Sr/Ba in barite across the Paleocene-Eocene Thermal Maximum: *Geology*,
505 v. 35, p. 1139-1142, doi: 10.1130/G24162A.1.

506 Piotrowski, A. M., Goldstein, S. L., Hemming, S. R., & Fairbanks, R. G., 2004. Intensification
507 and variability of ocean thermohaline circulation through the last deglaciation. *Earth and*
508 *Planetary Science Letters*, 225(1), 205-220.

509 Piotrowski, A.M., Goldstein, S.L., Hemming, S.R., & Fairbanks, R.G., 2005, Temporal
510 relationships of carbon cycling and ocean circulation at glacial boundaries. *Science*, v. 307,
511 p.1933-1938, doi.10.1126/Science.1104883.

512 Piotrowski, A. M., Goldstein, S. L., Hemming, S., Fairbanks, R. G., & Zylberberg, D. R., 2008.
513 Oscillating glacial northern and southern deep water formation from combined neodymium
514 and carbon isotopes. *Earth and Planetary Science Letters*, 272(1), 394-405.

515 Ridgwell, A., & Schmidt, D.N., 2010. Past constraints on the vulnerability of marine calcifiers
516 to massive carbon dioxide release. *Nature Geoscience*, v. 3., p. 196-200.

517 Röhl, U., Westerhold, T., Bralower, T.J., & Zachos, J.C., 2007, On the duration of the
518 Paleocene-Eocene thermal maximum (PETM). *Geochemistry Geophysics Geosystems*, v. 8,
519 Q12002.

520 Rutberg, R.L., Hemming, S.R., & Goldstein, S.L., 2000, Reduced North Atlantic Deep Water
521 flux to the glacial Southern Ocean inferred from neodymium isotope ratios. *Nature*, v. 405,
522 p. 935-938.

523 Scher, H.D., & Martin, E.E., 2006, Timing and climatic consequences of the opening of Drake
524 Passage. *Science*, v. 312, p. 428-430, doi.10.1126/Science.1120044.

525 Sluijs, A., Schouten, S., Pagani, M., Woltering, M., Brinkhuis, H., Damsté, J. S. S., Dickens, J.
526 & Moran, K., 2006. Subtropical Arctic Ocean temperatures during the Palaeocene/Eocene
527 thermal maximum. *Nature*, v. 441(7093), p. 610-613.

528 Sluijs, A., Brinkhuis, H., Schouten, S., Bohaty, S.M., John, C.M., Zachos, J.C., Reichart, G.-J.,
529 Sinninghe Damsté, J. S., Crouch, E.M., and Dickens, G.R., 2007, Environmental precursors
530 to rapid light carbon injection at the Palaeocene/Eocene boundary. *Nature*, v. 450, p. 1218-
531 1221.

532 Stichel, T., Frank, M., Rickli, J., & Haley, B.A., 2012, The hafnium and neodymium isotope
533 composition of seawater in the Atlantic sector of the Southern Ocean. *Earth and Planetary
534 Science Letters*, v. 317-318, p. 282-294.

535 Storey, M., Duncan, R.A., & Swisher, C.C., 2007, Paleocene-Eocene thermal maximum and the
536 opening of the northeast Atlantic. *Science*, v. 316, p. 587-589,
537 doi.10.1126/Science.1135274.

538 Svensen, H., Planke, S., Malthe-Sørenssen, A., Jamtveit, B., Myklebust, R., Eidem, T. R., &
539 Rey, S. S., 2004, Release of methane from a volcanic basin as a mechanism for initial Eocene
540 global warming. *Nature*, v. 429, p. 542-545, doi.10.1038/Nature02566.

541 Thomas, D.J., Zachos, J.C., Bralower, T.J., Thomas, E., & Bohaty, S., 2002, Warming the fuel
542 for the fire: Evidence for the thermal dissociation of methane hydrate during the Paleocene-
543 Eocene thermal maximum. *Geology*, v. 30, p. 1067-1070.

544 Thomas, D.J., Bralower, T.J., & Jones, C.E., 2003, Neodymium isotopic reconstruction of late
545 Paleocene-early Eocene thermohaline circulation. *Earth and Planetary Science Letters*, v
546 209, p. 309-322, doi.10.1016/S0012-821X(03)00096-7.

547 Thomas, D.J., 2004, Evidence for deep-water production in the North Pacific Ocean during the
548 early Cenozoic warm interval. *Nature*, v. 430, p. 65-68, doi.10.1038/nature02639.

549 Thomas, D.J., Lyle, M., Moore, T.C., & Rea, D.K., 2008, Paleogene deepwater mass
550 composition of the tropical Pacific and implications for thermohaline circulation in a
551 greenhouse world. *Geochemistry Geophysics Geosystems*, v. 9, doi.Q02002
552 10.1029/2007gc001748.

553 Thomas, D.J., Korty, R., Huber M., Schubert, J.A., Haines, B., 2014. Nd isotopic structure of
554 the Pacific Ocean 70-30 Ma and numerical evidence for vigorous ocean circulation and
555 ocean heat transport in a greenhouse world. *Paleoceanography*, **29**, 454–469,
556 doi:10.1002/2013PA002535.

557 Tripathi, A.K. & Elderfield, H., 2004, Abrupt hydrographic changes in the equatorial Pacific and
558 subtropical Atlantic from foraminiferal Mg/Ca indicate greenhouse origin for the thermal
559 maximum at the Paleocene-Eocene Boundary. *Geochemistry Geophysics Geosystems*, v. 5,
560 Q02006.

561 Tripathi, A. & Elderfield, H., 2005, Deep-sea temperature and circulation changes at the
562 Paleocene-Eocene thermal maximum. *Science*, v. 308, p. 1894-1898,
563 doi.10.1126/Science.1109202.

564 Wilson, D.J., Piotrowski, A.M., Galy, A., and McCave, I.N., 2012. A boundary exchange
565 influence on deglacial neodymium isotope records from the deep western Indian Ocean.
566 *Earth and Planetary Science Letters*, v 341-344, p 35-47. doi: 10.106/j.epsl.2012.06.009

567 Winguth, A., Shellito ,C., Shields, C., & Winguth, C., 2010, Climate Response at the Paleocene-
568 Eocene Thermal Maximum to Greenhouse Gas Forcing-A Model Study with CCSM3.
569 *Journal of Climatology*, v. 23, p. 2562-2584, doi.10.1175/2009jcli3113.1.

570 Zachos, J., Pagani, M., Sloan, L., Thomas, E., & Billups, K., 2001, Trends, rhythms, and
571 aberrations in global climate 65 Ma to present. *Science*, v. 292, p. 686-693.

572 Zachos JC, *et al.*, 2003, A transient rise in tropical sea surface temperature during the Paleocene-
573 Eocene Thermal Maximum. *Science*, v. 302, p. 1551-1554, doi.10.1126/Science.1090110.

574 Zachos, J.C., Röhl, U., Schellenberg, S.A., Sluijs, A., Hodell, D.A., Kelly, D.C., Thomas, E.,
575 Nicolo, M., Raffi, I., Lourens, L.J., McCarren, H., & Kroon, D., 2005. Rapid Acidification
576 of the Ocean During the Paleocene-Eocene Thermal Maximum. *Science*, v. 308, p. 1611-
577 1615.

578 Zachos, J. C., Schouten, S., Bohaty, S., Quattlebaum, T., Sluijs, A., Brinkhuis, H., Gibbs, S. &
579 Bralower, T. J., 2006. Extreme warming of mid-latitude coastal ocean during the Paleocene-
580 Eocene Thermal Maximum: Inferences from TEX86 and isotope data. *Geology* v. 34, no. 9,
581 p. 737-740.

582 Zachos, J.C., Dickens, G.R., & Zeebe, R.E., 2008. An early Cenozoic perspective on greenhouse
583 warming and carbon-cycle dynamics. *Nature*, v. 451, p. 279-283.

584 Zeebe, R.E. & Zachos, J.C., 2007, Reversed deep-sea carbonate ion basin gradient during
585 Paleocene-Eocene thermal maximum. *Paleoceanography*, v. 22, p. 3201.

586 Zeebe, R.E., Zachos, J.C., & Dickens, G.R., 2009, Carbon dioxide forcing alone insufficient to
587 explain Palaeocene-Eocene Thermal Maximum warming. *Nature Geoscience*, v. 2, p. 576-
588 580, doi.10.1038/ngeo578.

589

590

591

592

593

594

595 **Figure Captions:**

596

597 **Figure 1:** Nd and C isotope data (ϵ_{Nd} and $\delta^{13}\text{C}$) across the PETM from the Southern Ocean (a),
598 Pacific Ocean (b), and Atlantic Basins (c). The sediment leach ϵ_{Nd} are shown with circles and
599 solid lines; the fish teeth/debris ϵ_{Nd} from Thomas et al. (2003) are shown as dots. All data are
600 presented on directly comparable scales for both ϵ_{Nd} and $\delta^{13}\text{C}$. The sample ages are based on the
601 $\delta^{13}\text{C}$ age models. In (b) the age model of Site 1209B has been slightly adjusted (second x axis)
602 such that the $\delta^{13}\text{C}$ excursion coincides with the age of the PETM in the other cores. The shaded
603 vertical bar indicates the timing of the PETM as defined by the CIE in the cores.

604

605 **Figure 2:** Sediment leach ϵ_{Nd} and available fish teeth ϵ_{Nd} data from 55.1 to 55.4 Ma for all three
606 ocean basins. Sediment ϵ_{Nd} values are connected with a dotted line and fish teeth data are
607 represented by unconnected dots. The light green shaded area represents the PETM as defined
608 by the carbon isotope excursion from each core. The dark green shaded area reflects our
609 interpretation of the "trigger" timing.

610

611 **Figure 3:** A conceptual model of the intermediate/deep-water mixing changes across the PETM
612 as inferred from ϵ_{Nd} records of intermediate/deep-water mass geometries. Arrow boldness
613 reflects overturning circulation that could produce water mass geometries. Dashed arrows
614 represent weak overturning. *Italicized numbers* indicate an ϵ_{Nd} estimate interpreted from each site
615 for the time period. The time periods are broadly divided into a pre-PETM period, including all
616 data prior to the "trigger" as denoted in Figure 2; the "trigger" period which slightly precedes and
617 overlaps with the PETM; the PETM as defined by the CIE; and the post-PETM, including all

618 | [data after the CIE. Red arrows indicate interpretations that are more speculative as the data is](#)
619 | [not available.](#) The arrow directions reflect our interpretation of the general direction of flow, and
620 | are not meant to be viewed as precise flow-paths. The paleogeographic distribution of the
621 | continents is from Ocean Drilling Stratigraphic Network (ODSN).
622

623 **List of tables**

624

625 **Table 1:** Core information; all cores were collected as part of the [Deep Sea Drilling](#)
626 Program ([DSDP](#)) [and the Ocean Drilling Program \(ODP\)](#).

627 **Table 2:** Age Models

628 **Table 3:** Summary of neodymium isotope data

Figure 1

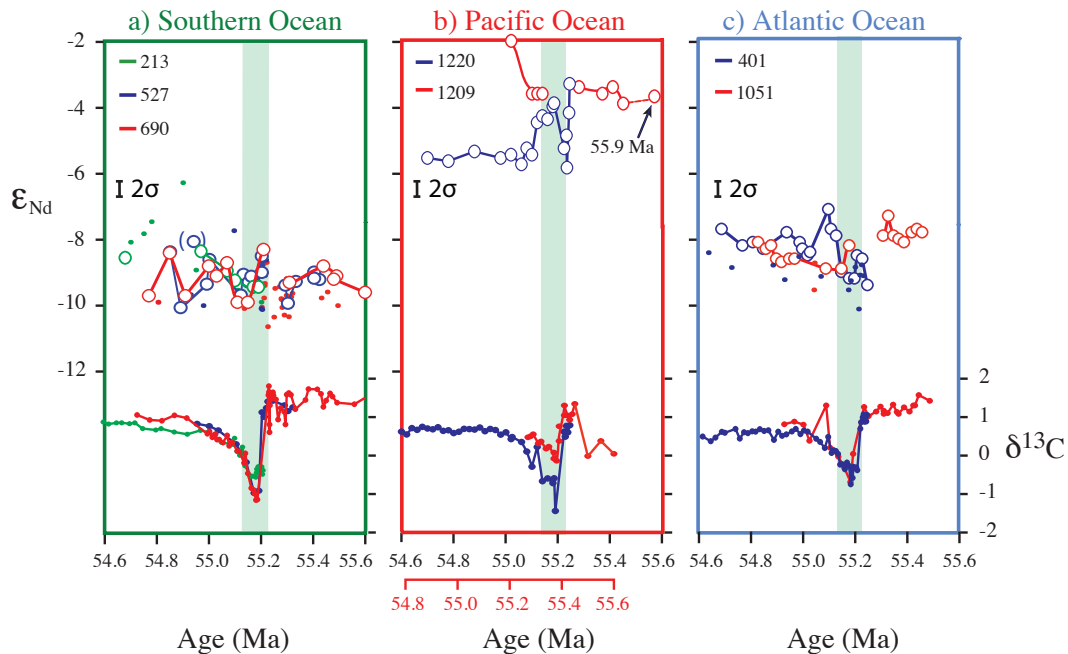


Figure 2

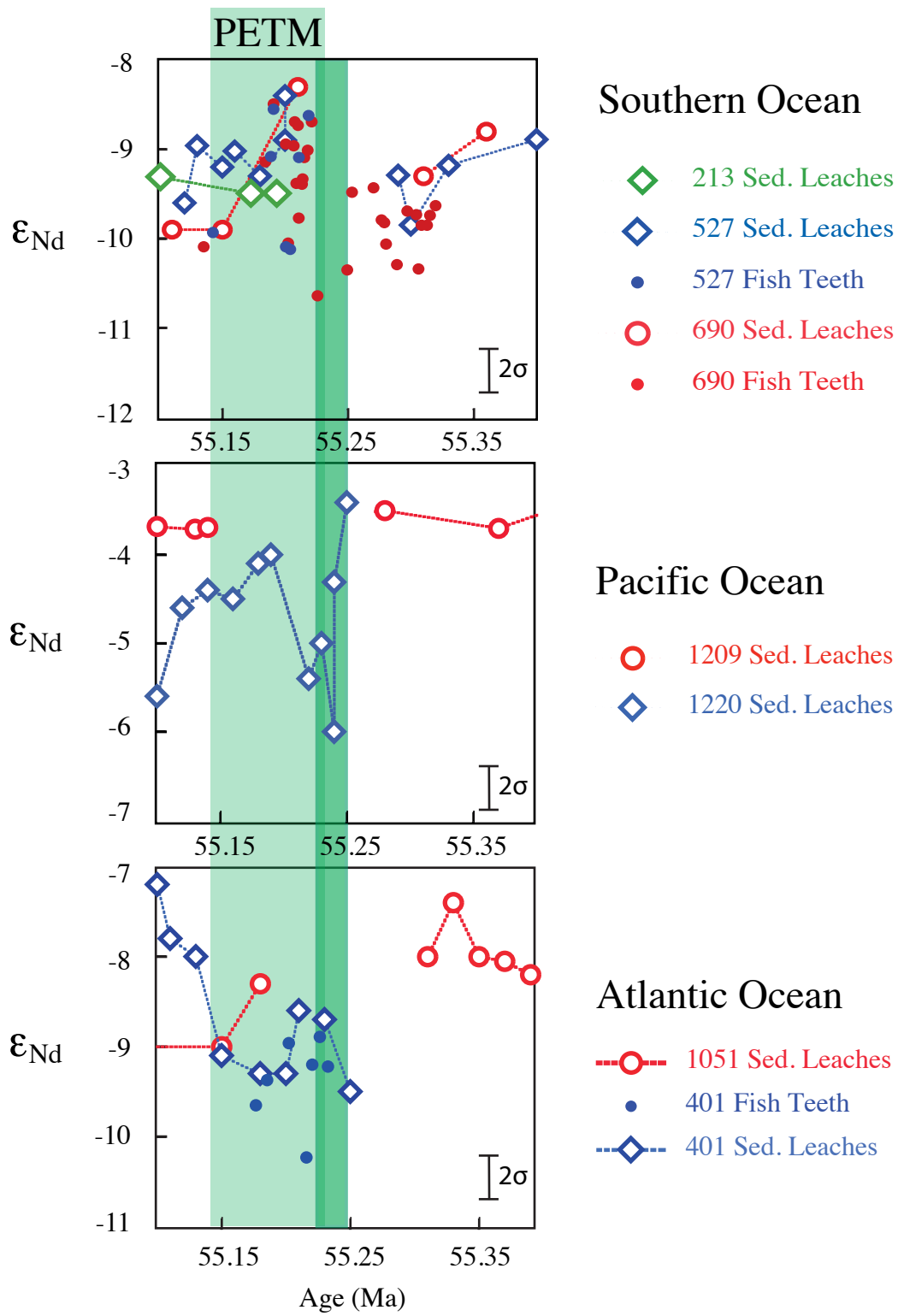


Figure 3

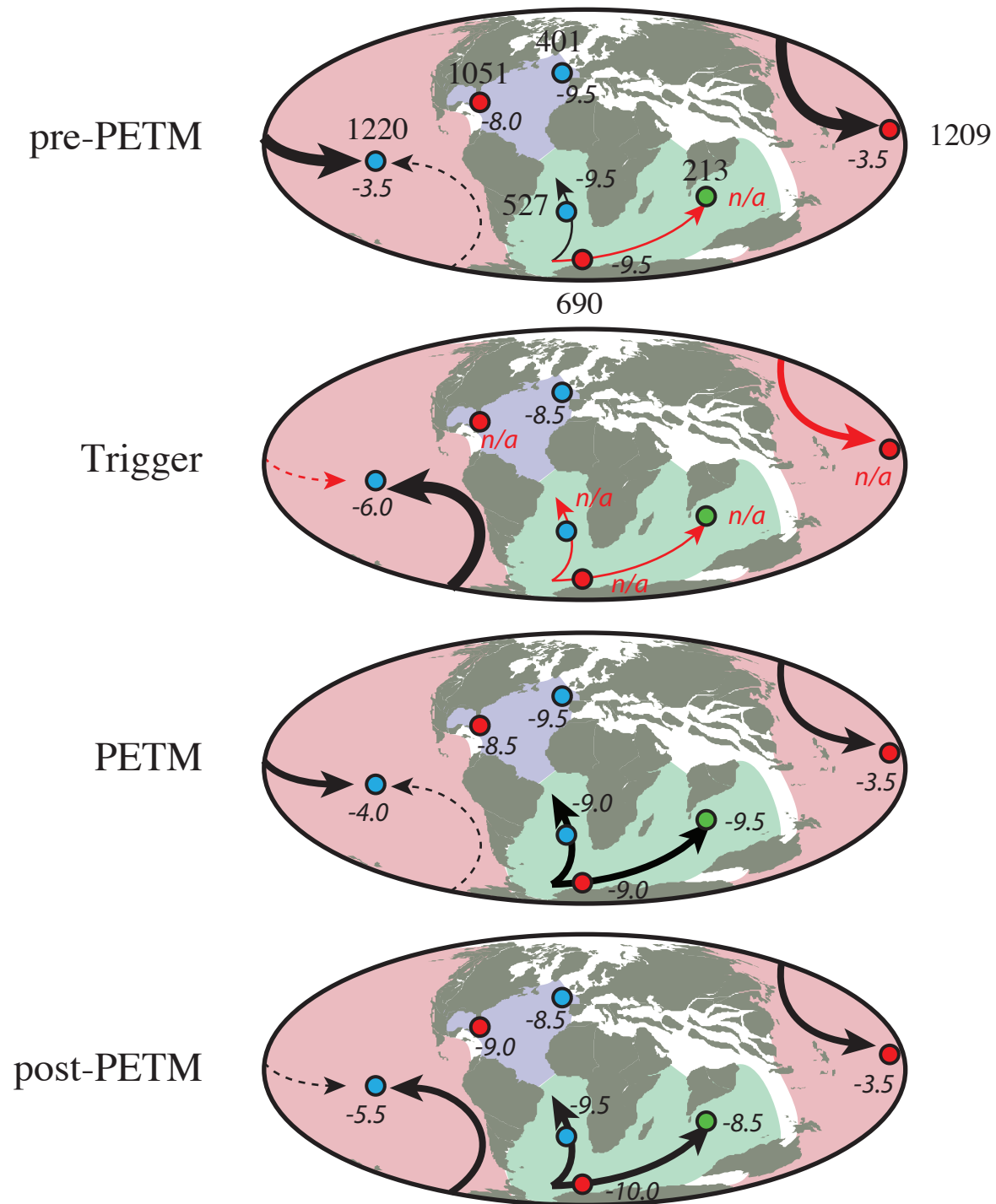


Table 1 Site Descriptions

Core	Modern Latitude and Longitude and depth (m)			Paleo-Depth (m)	$\delta^{13}\text{C}$ data reference
213	10°12.7'S	93°53.8'E	5601	3000	Thomas et al., 2003
401	47°25.7'N	8°48.6'W	2495	1900	Thomas et al., 2003
527	28° 2.5'S	1°45.8'E	4428	3400	Thomas et al., 2003
690B	65° 9.6'S	1°12.3'E	2914	1900	Thomas et al., 2003
1051B	30° 3.2'N	76°21.5'W	1981	2000	Thomas et al., 2003
1209B	32°39.1'N	158°30.4'E	2387	2400	Tripati and Elderfield, 2005
1220B	10°10.6'N	142°45.5'W	5218	3200	Tripati and Elderfield, 2005

Table 2 Sample Description and ϵ_{Nd}

Hole	Core Section	Depth Interval (cm)		ϵ_{Nd}	age Ma
		upper	lower		
1220B	20X-1	65	67	-5.70	54.70
1220B	20X-1	85	87	-5.80	54.78
1220B	20X-1	110	112	-5.50	54.88
1220B	20X-1	135	137	-5.70	54.98
1220B	20X-1	145	147	-5.60	55.02
1220B	20x-2	5	7	-5.90	55.06
1220B	20x-2	10	12	-5.40	55.08
1220B	20x-2	15	17	-5.60	55.10
1220B	20x-2	20	22	-4.60	55.12
1220B	20x-2	25	27	-4.40	55.14
1220B	20x-2	30	32	-4.50	55.16
1220B	20x-2	35	37	-4.10	55.18
1220B	20x-2	40	42	-4.00	55.19
1220B	20x-2	80	82	-5.40	55.22
1220B	20x-2	90	92	-5.00	55.23
1220B	20x-2	93	94	-6.00	55.24
1220B	20x-CCW	5	6	-4.31	55.24
1220B	20x-CCW	6	7	-3.41	55.25
1209B	22H-1	12	14	-2.10	55.02
1209B	22H-1	39	40	-3.88	55.10
1209B	22H-1	47	48	-3.71	55.13
1209B	22H-1	48	49	-3.69	55.14
1209B	22R-1	84	86	-3.50	55.28
1209B	22R-1	108	110	-3.70	55.37
1209B	22R-1	120	122	-3.50	55.41
1209B	22R-1	132	134	-4.00	55.45
1209B	22R-1	148	150	-3.70	55.85
0690B	18H-5	36	37	-9.70	54.77
0690B	18H-6	30	31	-8.40	54.84
0690B	18H-6	110	111	-9.70	54.91
0690B	19H-1	30	31	-8.80	55.00
0690B	19H-1	65	66	-9.10	55.03
0690B	19H-1	137	138	-8.70	55.07
0690B	19H-2	47	48	-9.90	55.11
0690B	19H-2	109	110	-9.90	55.15
0690B	19H-3	69	71	-8.30	55.21
0690B	19H-4	66	67	-9.30	55.31
0690B	19H-5	6	7	-8.80	55.36
0690B	19H-5	65	66	-9.10	55.44
0690B	19H-5	106	107	-9.20	55.48
0690B	20H-1	3	4	-9.63	55.53
0690B	20H-1	140	141	-9.84	55.80
0690B	20H-2	111	112	-9.20	56.17
527	24R-1	11	12	-8.27	54.85
527	24R-1	31	32	-9.98	54.89
527	24R-1	53	54	-7.95	54.94
527	24R-1	81	82	-9.26	54.99
527	24R-1	100	102	-8.50	55.00
527	24R-1	140	142	-9.60	55.12
527	24R-2	11	12	-8.96	55.13
527	24R-2	41	42	-9.20	55.15
527	24R-2	87	88	-9.02	55.16
527	24R-2	24	27	-9.30	55.18
527	24R-2	30	33	-8.90	55.20
527	24R-2	47	48	-8.40	55.20
527	24R-3	59	60	-9.29	55.29
527	24R-3	81	82	-9.85	55.30
527	24R-3	121	122	-9.18	55.33
527	24R-4	10	11	-8.89	55.40
527	24R-4	40	41	-9.12	55.42
527	24R-4	80	81	-9.08	55.40
213	16-3	48	49	-8.60	54.69
213	16-4	8	9	-8.40	54.97
213	16-4	49	50	-9.00	55.08
213	16-4	58	59	-9.30	55.10
213	16-4	90	91	-9.50	55.17
213	16-4	99	100	-9.50	55.19
1051B	59X-2	110	111	-8.23	54.50
1051B	59X-2	139	140	-8.41	54.60
1051B	59X-3	26	27	-8.26	54.76
1051B	59X-3	46	47	-8.65	54.80
1051B	59X-3	67	68	-8.81	54.90
1051B	59X-3	87	88	-8.75	54.94
1051B	59X-3	120	120	-8.70	54.97
1051B	60X-1	65	65	-9.00	55.09
1051B	60X-1	119	120	-9.00	55.15
1051B	60X-1	145	145	-8.30	55.18
1051B	60X-2	56	56	-8.00	55.31
1051B	60X-2	64	66	-7.40	55.33
1051B	60X-2	74	75	-8.00	55.35
1051B	60X-2	84	85	-8.05	55.37
1051B	60X-2	93	94	-8.20	55.39
1051B	60X-2	109	110	-7.89	55.42
1051B	60X-2	118	119	-7.79	55.44
1051B	60X-2	142	143	-7.93	55.52
401	14R-1	45	47	-7.80	54.69
401	14R-1	100	101	-8.26	54.77
401	14R-1	125	126	-8.24	54.81
401	14R-1	146	147	-8.40	54.85
401	14R-2	50	52	-7.90	54.94
401	14R-2	83	85	-8.20	54.99
401	14R-2	91	93	-8.40	55.00
401	14R-2	100	102	-8.60	55.02
401	14R-2	110	112	-8.50	55.03
401	14R-2	148	150	-7.20	55.10
401	14R-3	6	8	-7.80	55.11
401	14R-3	21	23	-8.00	55.13
401	14R-3	31	33	-9.10	55.15
401	14R-3	52	54	-9.30	55.18
401	14R-3	84	86	-9.30	55.20
401	14R-3	90	92	-8.60	55.21
401	14R-3	122	124	-8.70	55.23
401	14R-3	148	150	-9.50	55.25

Table 3 Age model description

Core	Age model segment	Core depth (MBSF)		Curve definition	
		start	end	m	b
1209B	a	210.72	211.24	0.3539	-19.317
	b	211.26	211.40	2.5000	-472.660
213	a	145.13	147.35	0.2541	+17.727
	b	147.41	147.64	0.1193	+37.590
401	a	198.54	201.97	0.1640	+22.054
	b	202.02	202.98	0.0656	+41.922
1220B	a	197.55	199.20	0.4009	-24.697
	b	199.25	199.93	0.0955	+36.159
527	a	199.63	200.71	0.2027	+14.491
	b	200.89	202.76	0.0700	+41.129
690B	a	162.80	170.69	0.0646	+44.199
	b	170.71	170.76	0.0453	+47.528
	c	170.84	172.49	0.1923	+22.416
	d	172.95	179.80	0.1167	+35.192
1051B	a	510.17	512.35	0.1164	-4.439
	b	512.40	513.80	0.2100	-52.412